Residual Stress Induced Mechanical Property Enhancement in Steel Encapsulated Light Metal Matrix Composites

Sean Fudger[a,b1], Dimitry Sediako[c2], Prashant Karandikar[d3], Chaoying Ni[a*]

[a]Department of Materials Science and Engineering, University of Delaware, 201 Du Pont Hall, Newark, DE 19716-1501, USA.
[b]Army Research Laboratory, Aberdeen Proving Ground, MD 21005, USA
[c]Canadian Neutron Beam Centre, Canadian Nuclear Laboratories, Chalk River, ON K0J 1J0 Canada
[d]M Cubed Technologies, Inc., 1 Tralee Industrial park, Newark, DE 19711, USA

fudgersj@udel.edu

dimitry.sediako@cnl.ca

prashant.karandikar@ii-vi.com

cni@udel.edu

[*]Corresponding author: Chaoying Ni. 1(302)831-6359

Abstract
Macro hybridized systems consisting of steel encapsulated metal matrix composites (MMCs) were produced with the goal of creating a low cost/light weight system with enhanced mechanical properties. The systems exhibit the high strength and modulus commonly expected from steels and high specific stiffness and low density observed in MMCs. The material combination also works to alleviate the high density of steels and the poor ductility of the MMCs. Furthermore, a coefficient of thermal expansion (CTE) mismatch induced residual compressive stress method is utilized to improve the ductility of the MMCs. Systems consisting of an A36 or 304 stainless steel shell with an Al-SiC or Al-Al_2O_3 shell are evaluated via neutron diffraction to quantify bulk residual stresses. The analysis shows variation in the measured strain due to steel thickness, difference in CTE between materials, and position within the composite. Improvements in ductility and yield stress are a result of these strains.

Keywords: Metal-matrix composites (MMCs); Mechanical properties; Residual/internal stress

1. Introduction

A high demand exists in the aerospace, marine, and automotive industries for components which are light weight but maintain their structural integrity under conditions of applied tension, compression, or torsion [1]. Recent interest includes materials such as high strength composites, magnesium, aluminum, steel, and combinations in the form of metal matrix composites and hybrid structures [2]. Metal matrix composites have a wide range of applicability for automotive and structural applications due to the ability to easily adjust the physical and/or mechanical

[1] 1(518)637-2059
[2] 1(613)639-2029
[3] 1(302)454-8600

properties [3], [4]. Furthermore, particulate reinforced aluminum or magnesium based MMCs which contain a sufficiently high volume fraction of ceramic reinforcement can provide the very high stiffness, low CTE, and low density expected in ceramics but still preserve the processing advantages of cast light metals. Many mechanical and physical properties can be manipulated by adjusting the size, distribution, or volume fraction of the reinforcement phase, utilizing different reinforcement materials, changing the matrix alloy, or adjusting the processing parameters used in fabricating the MMCs [5]–[7].

The objective of this research is to develop a low cost/light weight macro composite materials system with increased specific stiffness, increased strength, increased damage tolerance, reduced density, and greater structural efficiency. A number of macro composite material systems were mechanically tested and evaluated via neutron diffraction. Each system includes an MMC core consisting of either an Al-10Si matrix alloy reinforced with particulate silicon carbide (SiC) or an Al-4Mg matrix alloy reinforced with particulate alumina (Al_2O_3). As undesirable thermodynamic instabilities exist, matrix alloys were chosen to mitigate the effects. Since SiC tends to form Al_4C_3 when it reacts with aluminum, Al-10Si was chosen to avoid the formation of Al_4C_3 and subsequent degradation of the reinforcement particles which can drastically diminish mechanical properties [7]. An Al-4Mg alloy was selected for use with the Al_2O_3 reinforcement since this alloy exhibits better ductility. Two steels are evaluated in this work: A36 steel and 304 stainless steel, which have significantly different mechanical properties and CTE. By selecting a steel with a higher coefficient of thermal expansion than its MMC core, a residual compressive stress is introduced onto the core due to contraction of the steel upon cooling from processing temperatures. The ability to tailor a metal matrix composite's CTE by adjusting the reinforcement percentage allows the selection of CTE mismatch to be chosen which results in sufficient residual strain on the MMC to improve mechanical properties. Liu and Lewandowski showed a hydrostatic pressure of 300 MPa (43.5 ksi) increased the reduction of area from 10 % to 80 % and quadrupled failure strain in a 6061 aluminum alloy reinforced with 15 vol% Al_2O_3 particulates [8], [9]. Neutron diffraction was performed as a means of measuring bulk material strains and calculating stresses within both the steel and MMC materials.

2. Experimental Procedure

The steel encapsulated metal matrix composites produced for this work are formed by casting or infiltrating a molten MMC into a steel shell. The casting/infiltration processes require no additional filler material, can be incorporated into complex geometries, and are produced at a relatively low cost [10], [11]. Steel/MMC macro hybridized cylindrical rods and cylindrical dog-bone tensile bars were produced by M-Cubed Technologies Inc. Newark DE. Steel bars (A36 and 304) with a diameter of 0.625”, 0.875” or 1.00 were bored to produce a tube with an inside diameter of 0.375”. The hollow steel tubes were then filled with Al-10Si reinforced with particulate Al-SiC or Al-4Mg reinforced with particulate Al-Al_2O_3. The various MMC core diameters remained constant at 0.375” but are surrounded by 3 different thicknesses of steel to provide for 3 different residual stress conditions [10]–[14]. A similar process was used to produce cylindrical dog-bone tensile samples as per ASTM B557-10. However these samples exhibit an inner diameter of 0.188" and had their gauge diameters turned down to 0.300”, 0.400”, or 0.500.”

2.1 Neutron Diffraction

Neutron diffraction is utilized as a means of directly measuring through thickness strain profiles in each phase of the macro hybridized cylindrical rods. The neutron diffraction measurement technique allows for measurement of large gauge volumes (1x1x10mm rectangular prism for this work), significant depth of penetration; up to 30 mm in steels and 250 mm in aluminum, and can separate stress contributions from each phase within the hybrid composites [15]. Similar to traditional x-ray diffraction, neutron diffraction follows Bragg's law (1):

$$n\lambda = 2d\sin(\theta) \quad (1)$$

The incident neutron beam penetrates the sample, interacting with crystals in its path. Various crystallographic planes diffract the beam to characteristic 2θ angles based on the atomic spacing of the material. Here *d* is the spacing between diffracting *hkl* planes, θ is the diffraction angle, *n* is an integer, and λ is the wavelength of the monochromatic neutron beam. Determination of strain within a material requires measurement of a stress-free "standard" for quantification. In equation (2), ε is strain, d is the measured atomic spacing of the sample, and d_0 is the measured atomic spacing of the stress-free "standard."

$$\varepsilon = \frac{d-d_0}{d_0} \quad (2)$$

The source of the observed strains varies greatly with the composite material constituents. Generally speaking, they can be divided into 3 categories based on the length scale over which the strain acts. Type I stresses, also called macro-stress and engineering stress, typically fluctuate on a length scale proportional to many grains (several millimeters in size). These stresses are often the result of the fabrication method including the processing parameters, phase constituents and structural geometry. Type II stresses typically fluctuate on a length scale proportional to individual grains. These stresses result from inhomogeneity within a material or between phases in a composite; specifically a coefficient of thermal expansion (CTE) mismatch, elastic modulus mismatch, or discontinuity in plastic flow resulting from elastically deforming particles. Type III stresses fluctuate over the smallest distances down to atomic length scales. These stresses can result from variations in local stress fields around dislocations [16]. Type-I and Type-II stresses contribute to the shifts in the positions of diffraction lines and Type-II and Type-III stresses contribute to diffraction line-widths [15].

All neutron diffraction measurements were performed at the Canadian Neutron Beam Centre, (CNBC) of the Canadian Nuclear Laboratories in Chalk River, Ontario, utilizing the L3 diffractometer. (115) reflection of a single crystal Ge monochromator was used to filter the spectrum resulting in a beam of neutrons that possess a narrow energy band exhibiting a wavelength of 1.5509 Å.

Stress-free "standards" were fabricated in the form of rectangular prisms, approximately 2x2x20mm in size, similar in appearance to match-sticks. In an effort to limit the amount of residual stress introduced during fabrication of these specimens, electrical discharge machining was utilized. Since there is no direct contact between the tool and sample, machining is performed without introducing additional mechanical stresses which result from traditional cutting methods. Samples were fabricated for each of the steels and unreinforced Al-10Si and Al-4Mg alloys. In addition, equivalent match-sticks were made from powder SiC and Al_2O_3.

The raw powder reinforcements were poured into a vanadium crucible so a similar gauge volume could be measured. Vanadium is typically used as a container material since its nuclei hardly scatter neutrons due to low coherent scattering length and large incoherent cross section, resulting in a flat background that has no effect on the diffraction peaks of the powders. The average stress-free d_0 was measured from each of these samples with a gauge volume of 1x1x10 mm to be used for the corresponding strain calculations.

For each sample, limited by geometry, there are three measurement areas within the steel shell and four measurement areas within the MMC core. Since the steel thickness varied between the samples, step sizes were chosen such that they represent even spacing between measurements and span the thickness of the steel wall. The first measurement is ½ step size inside the outer diameter of the steel and subsequent measurements penetrate deeper into the material. This process is repeated for the MMC core except the final measurement is in the center of the MMC, see figure 1. Since the core is a composite consisting of an aluminum alloy and reinforcement particles, separate measurements are made at each MMC location since each of the constituent materials diffracts at different angles and will be subjected to different strains. The following miller indices were used for strain measurement in their respective phases: ferrite (211), austenite (111), Al-10Si (311), Al_2O_3 (211), and SiC (110), Al-4Mg (311) and (220). (220) reflection of Al-4Mg was used in addition to (311) because peak shouldering or secondary peak formation was observed in close proximity to (311) peak.

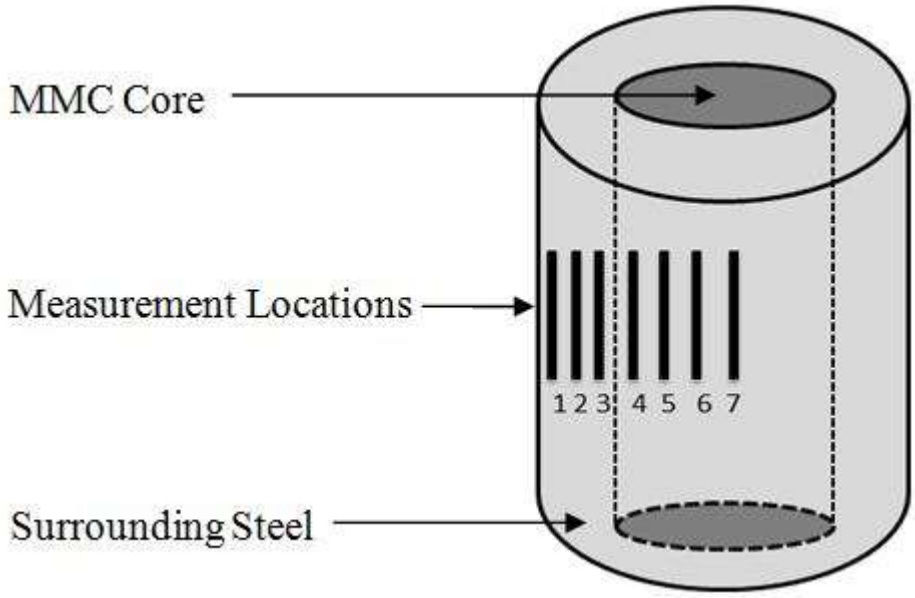

Figure 1. Diagram of the measurement locations on a hybrid-composite; Locations 1-3 are within the steel, 4-7 are within the MMC core.

It is necessary to measure three separate orientations, axial, radial, and hoop for the cylindrical geometry, to properly map the stresses within the sample. For example, equation (3) solves for stress, σ, where E is Young's Modulus, ν is Poisson's ratio, and ε is strain as measured from equation (2). Subscripts A, R, and H represent axial, radial, and hoop directions respectively.

$$\sigma_A = \frac{E}{1+\nu}\left[\varepsilon_A + \frac{\nu}{1-2\nu}\left(\varepsilon_A + \varepsilon_R + \varepsilon_H\right)\right] \quad (3)$$

The measurement gauge volume was maximized to decease the required collection time and associated error. Radial and hoop measurements were performed with a 1mm by 10mm beam slit whereas the axial measurement was limited to a 1mm by 1mm beam slit due to geometry. Although measuring a larger area may be more representative of the bulk material condition, the smaller beam geometry is still capable of obtaining narrow peaks with a high signal to noise ratio, see figure 2, when the collection time is increased. A 32 line detector with 0.1-degree angular resolution was used to capture the diffracted beam resulting in the 3.2 degree collection width observed in figure 2.

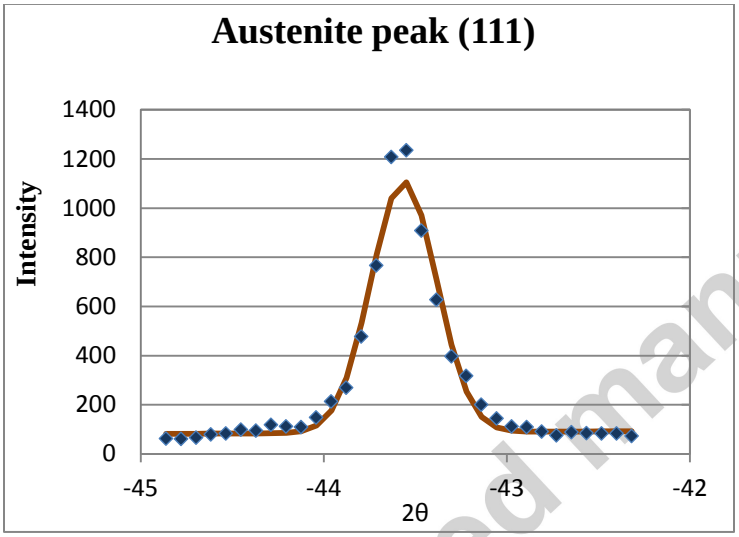

Figure 2. Example of a typical Bragg peak (with Gaussian distribution) measured in 304 SS.

Throughout the set of experiments, each sample must be examined with exactly the same calibrated set-up, wavelength, collimators and slits as the reference standards. Furthermore, the alignment of the beam and position of the samples is also a crucial step in guaranteeing accurate results. First, the sample is lined up optically to establish a datum, typically the edge of the cylindrical sample. This step is then followed by a second alignment, this time utilizing the count rate of the neutrons to more accurately determine the samples position relative to the path of the beam.

Figure 3 shows the steady-state neutron diffraction setup utilized at the Chalk River site for strain measurement. The current configuration illustrated in Figure 3b is set up to measure the hoop direction on 3 macro-composite specimens.

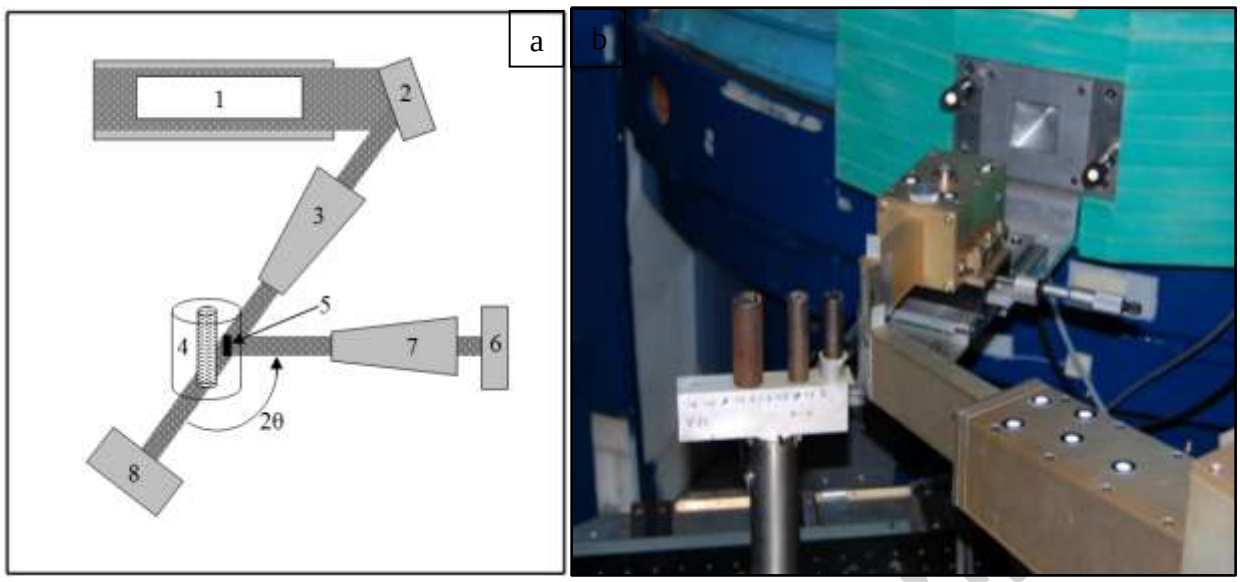

Figure 3. a) Schematic [17] b) photo of steady-state neutron diffraction setup for strain measurement.

1. Neutron beam source
2. Single crystal germanium monochromator resulting in a 1.5509 Å wavelength.
3. Beam defining optics: collimator and cadmium slit to shape incident beam
4. Specimen(s)
5. Interaction volume
6. Detector
7. Beam defining optics: collimator and cadmium slit to shape diffracted beam
8. Beam stop: lead shielding

2.2 Mechanical Testing

Tensile testing was performed on the cylindrical dog-bone tensile samples as per ASTM B557-10, see tensile specimen schematic in figure 4.

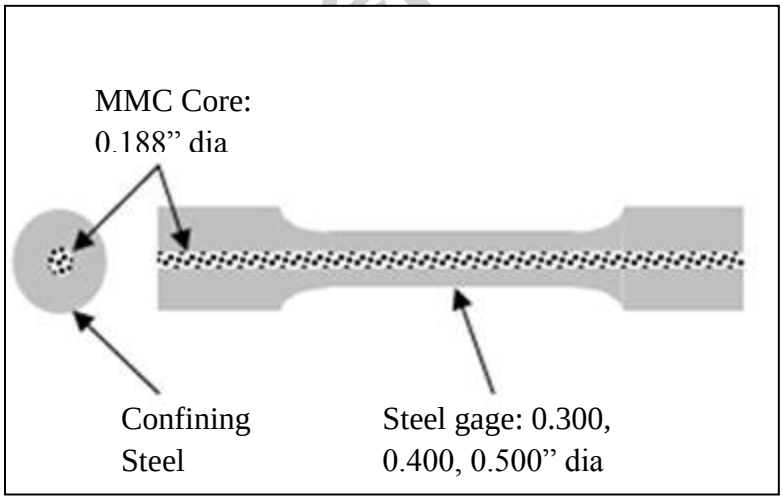

Figure 4. Schematic of macro composite tensile specimen [11].

Two identical samples for each macro composite system configuration were tested and the average value reported with standard error reported as error bars. To accurately compare the various steel/MMC macro hybridized systems, the specific properties were calculated. For example, specific stress is the stress divided by the density of the material system in question. By comparing specific properties one can account for density differences between the steels and MMC systems. Since the volume fraction of reinforcement and different steel thicknesses affect the density of the system, specific properties allow for a normalized comparison. The %MMC refers to the ratio between the area of MMC core to the total area of the hybrid system (MMC + steel). The specific properties of the monolithic steel are plotted at 0 % MMC while the specific properties of the MMC are indicated at 100%. The mechanical properties of the steels and the MMCs have been measured independently from dog-bone tensile specimens. The dashed line between these points represents a linear rule of mixtures (ROM) prediction. The ROM allows for an estimation of how different proportions of steel and MMC will behave as a composite system. The results from mechanical testing are presented in figure 9.

3. Results and Discussion

During processing, the hollow steel rods are heated to a processing temperature between 600 and 750 °C. At these temperatures, the molten MMCs are cast or infiltrated inside the hollow cavity created in the steel. Upon cooling the materials attempt to shrink proportional to their coefficient of thermal expansion. Evident from literature for 2009Al-25 vol% SiC_p [18], 2124Al-17 vol% SiC_p [19], and 6061Al-15 vol% SiC_w [20] thermal residual stresses due to a CTE mismatch between the phases results in tension in the matrix and compression in the reinforcement when MMC's are cooled from processing temperatures. The ceramic particles have a substantially lower CTE compared to the aluminum matrix, 3 and 6 for SiC and Al_2O_3 respectively vs. 23 ppm/K for both aluminum matrix alloys, see table I. The aluminum attempts to shrink around the reinforcement particle, upon doing this, the aluminum transfers a load onto the particle. Due to the high stiffness of the ceramic particle, it does not necessarily yield of break but imparts a residual compressive stress on the particle. At the same time, the forces balance on the aluminum which can result in yielding and plastic deformation within the matrix, leading to residual tensile stress. CTE mismatch in MMCs is accepted in literature as a means of increasing dislocation density and thus increasing yield stress and ultimate tensile stress in the composite [21]–[23].

Table I. Material properties.

Material	Matrix	Vp	E (GPa)	ν	CTE (ppm/K)
A36	N/A	N/A	200	0.26	11.7
304 SS (annealed)	N/A	N/A	200	0.29	16.6
Al-10Si	N/A	N/A	66	0.35	23
Al-4Mg	N/A	N/A	69	0.36	23
Hot Pressed SiC	N/A	N/A	453	0.19	3
Al_2O_3	N/A	N/A	370	0.22	6
Al/Al_2O_3	Al-4Mg	46	160	0.29	11.2
Al/SiC	Al-10Si	30	120	0.29	15.6

Al/SiC	Al-10Si	55	202	0.25	11.8

Vp – particle volume fraction, E – Young's modulus; ν - Poisson's ratio; CTE – coefficient of thermal expansion (20-100ºC). Sources: M Cubed Technologies (MCT) [24] or directly from the manufacturer's websites or datasheets [25], [26].

3.1 Neutron Diffraction

Neutron diffraction measurements were performed on each of the macro composite materials systems. It is clear that the type II stresses do not normally average to zero in each phase and thus, like the macro stress, cause a shift in the Bragg scattering angles which allows the average strain in each phase over the sample gauge volume to be measured. Figure 5 presents the results of residual stress calculations using equation (3) for the A36 and 304 stainless steels, each with the Al-SiC 55P MMC and varying outer steel thicknesses.

Since the core is a composite of two materials: matrix and reinforcement, the strains were measured separately. The MMC core diameter is the same for all materials however the outer steel thickness varies according to the chart title. It can be seen that within the respective material systems, a thicker outer steel diameter results in a higher magnitude of residual compressive stress in the SiC reinforcement particles.

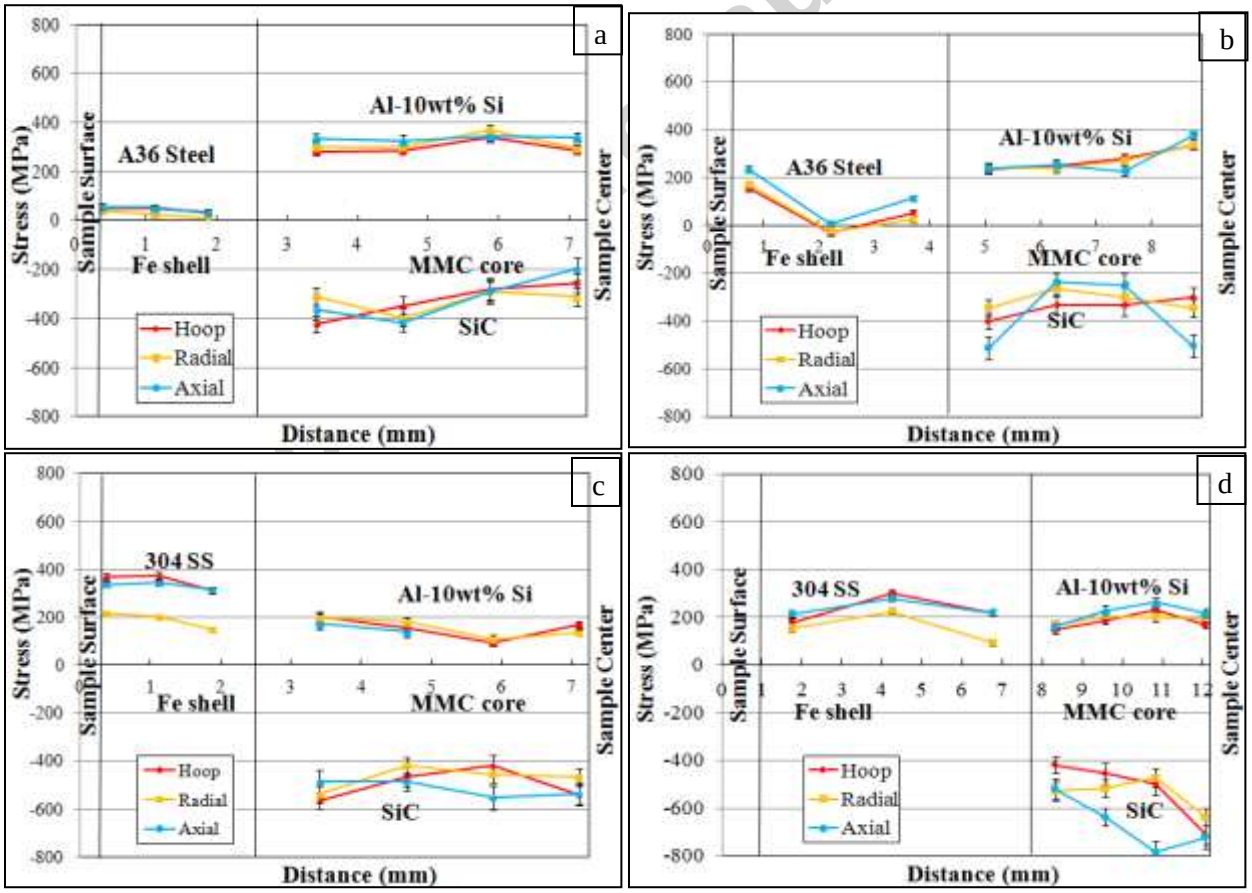

Figure 5. Neutron diffraction residual stress results a) A36/Al-SiC 55P 0.626" steel outer diameter b) A36/Al-SiC 55P 0.875" c) 304/Al-SiC 55P 0.626" d) 304/Al-SiC 55P 1.0."

Furthermore, an additional strain is applied to the MMC core via the steel encapsulant. The surrounding steel contracts onto the MMC core affecting the residual stresses based on the CTE mismatch. Considering the MMC as having one averaged value of CTE based on the volume percentage of its constituents the following trends can be observed. Since the CTE is comparable between the A36 steel and the Al-SiC 55P, the residual stresses observed on the MMC are dominated by the Al-SiC CTE mismatch. The weak confinement offered by the A36 steel has little effect on the observed stresses on the core. Conversely, the 304 SS with the Al-SiC 55P samples have a much higher CTE difference. The surrounding 304 SS contracts around the MMC compressing both the matrix and reinforcement. Lower tensile values are observed in the aluminum matrix and higher compressive values are observed in the SiC reinforcement. The effect of the steel can be isolated since the MMC core is identical between the samples and the elastic constants between the steels are comparable. This indicates the type II thermal misfit stresses are the dominant stress type present in these materials.

Figures 6-8 present the neutron diffraction residual stress results for the remaining systems: A36 Al-Al_2O_3 46P 1.0", A36 Al-Al_2O_3 46P 0.626", 304 Al-Al_2O_3 46P 1.0", 304 Al-Al_2O_3 46P 0.626", 304 Al-SiC 30P 1.0", and 304 Al-SiC 30P 0.626" respectively. Consistent with the previous neutron diffraction data, thicker surrounding steel results in lower tensile stress in the aluminum matrix and higher compression in the reinforcement when compared to thinner steel for each system.

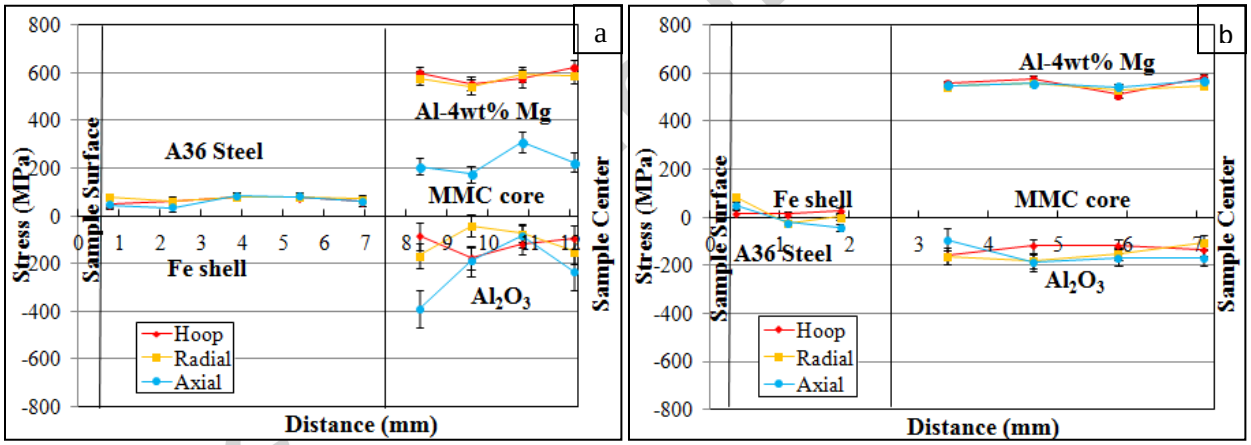

Figure 6. Neutron diffraction residual stress results in A36/Al-Al_2O_3 46P a) 1.0" outer steel diameter, b) 0.626" outer steel diameter.

The higher CTE mismatch offered in the 304 Al-Al_2O_3 46P compared to the A36 Al-Al_2O_3 46P systems results in higher magnitude compression in the reinforcements and also compressive stress in the matrix. The additional confinement from the steel brings the entire core into compression.

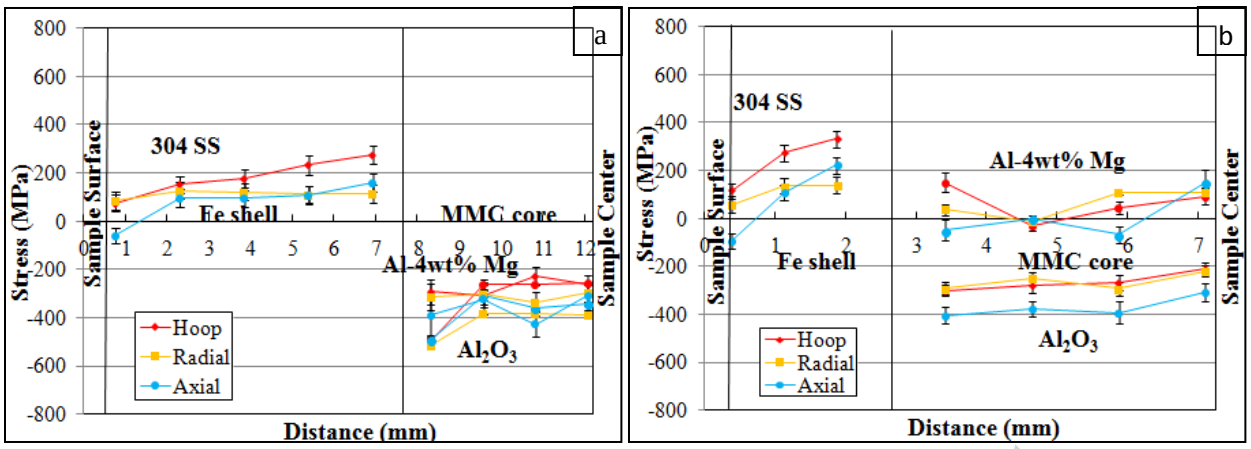

Figure 7. Neutron diffraction residual stress results in 304/Al-Al_2O_3 46P a) 1.0" outer steel diameter, b) 0.626" outer steel diameter.

Lower magnitude residual compressive stresses are observed in the Al_2O_3 compared to the SiC reinforcements. This is attributed to a substantially lower Young's modulus (E), see table I, for Al_2O_3 compared to SiC. Even in the case of a low CTE mismatch system with SiC reinforcement, namely 304 Al-SiC 30P, it still exhibits drastically higher residual compressive stresses in the reinforcement than a high CTE mismatch system reinforced with alumina, 304 Al-Al_2O_3 46P. Furthermore, it can be seen that the lower stiffness of the Al_2O_3 results in less load taken on the reinforcement, thus as the loads balance higher magnitude residual stresses are observed in the matrix.

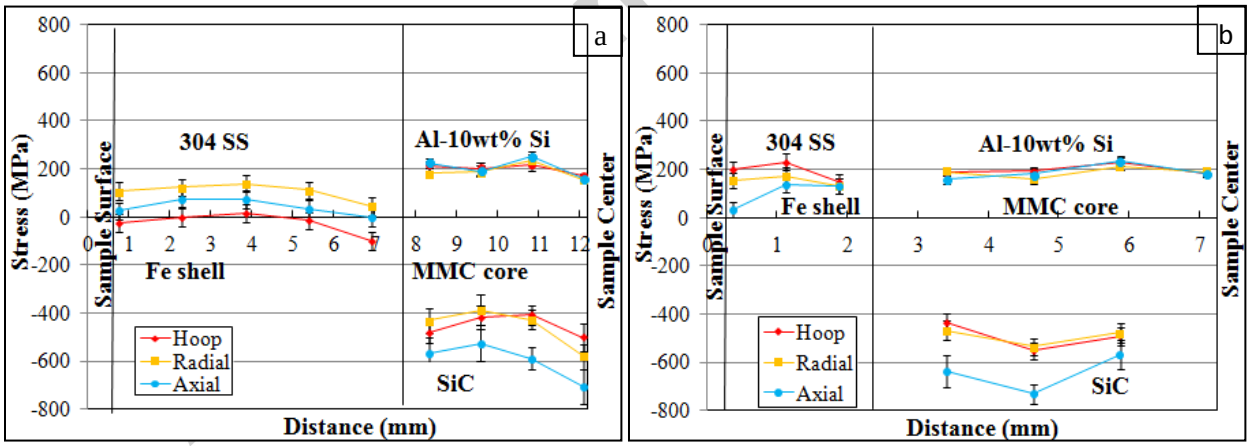

Figure 8. Neutron diffraction residual stress results in 304/Al-SiC 30P a) 1.0" outer steel diameter, b) 0.626" outer steel diameter.

Comparable magnitude residual stresses are observed in the 304 Al-SiC 30P and 304 Al-SiC 55P despite having drastically different CTE mismatches, 1.0 and 4.8 ppm/K respectively. When considering the different reinforcement percentages, 30 volume percent and 55 volume percent, it can be seen that less of the MMC material volume is in compression in the 30P case. While the magnitudes seem comparable for each phase, evaluating the composite material as a sum of its proportional components yields a composite stress nearly 200 MPa further in compression. The observed increase in the MMCs residual compressive stress is a direct result of the additional confinement caused by the larger CTE mismatch.

Uncertainty in the strain measurement and the resulting stress calculation is a result of many factors relating to the measurement and reference values and include: uncertainty in the measurement of d and d_0, the incident beam wavelength, and the measurement position within the specimen.

3.2 Mechanical Testing

Figures 9a and 9b present specific yield stress and specific ultimate tensile stress vs. % MMC. Evident from the data compared to the rule of mixture predictions (dotted lines), the systems which see the most improvement are those surrounded by the 304 stainless steel. Minor improvements are observed in the ultimate tensile strength at all steel shell thicknesses. Furthermore, substantially larger improvements are seen in yield strength for the conditions in which thicker steel shells are present. An improvement in the yield stress and ultimate tensile stress is a result of successful load transfer from the compliant matrix to the stiff reinforcement particles. Furthermore, an increased flow stress resulting from additional dislocations in the matrix is a direct result of superposed pressure [27].

Conversely, each of the systems containing A36 steel, regardless of the reinforcement type see a substantial drop in both specific yield stress and specific ultimate tensile stress. Failure occurs via brittle intergranular fracture within the matrix and none of the reinforcement particles appear to have cracked. In this case, there appears to be no advantage to the hybridized system.

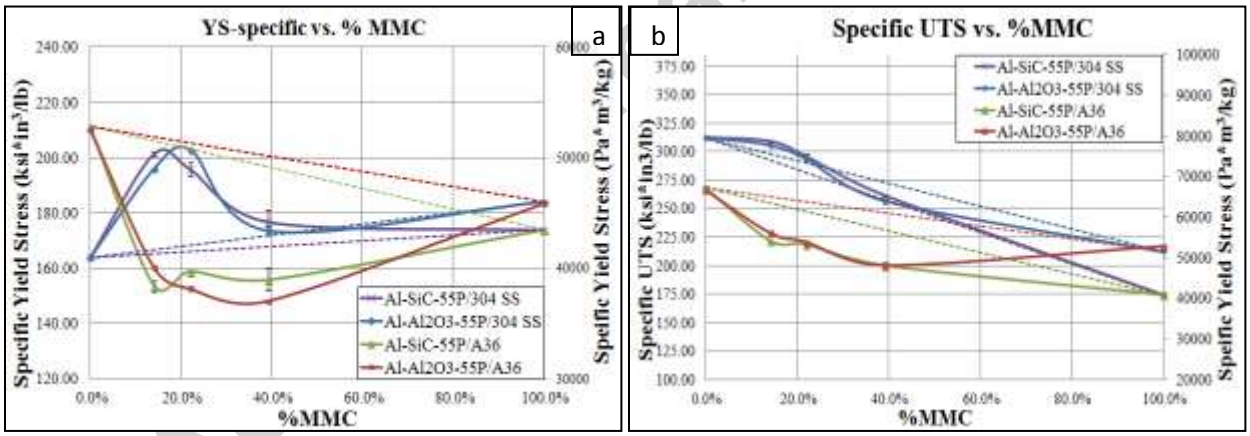

Figure 9. (a) Specific yield stress vs. % MMC (b) Specific ultimate tensile stress vs. % MMC for each macro composite materials system.

Cracking of the reinforcement particles, see figure 10a, along with a high residual compressive stress measured within the reinforcement phase is indicative of successful load transfer and good bonding with the matrix.

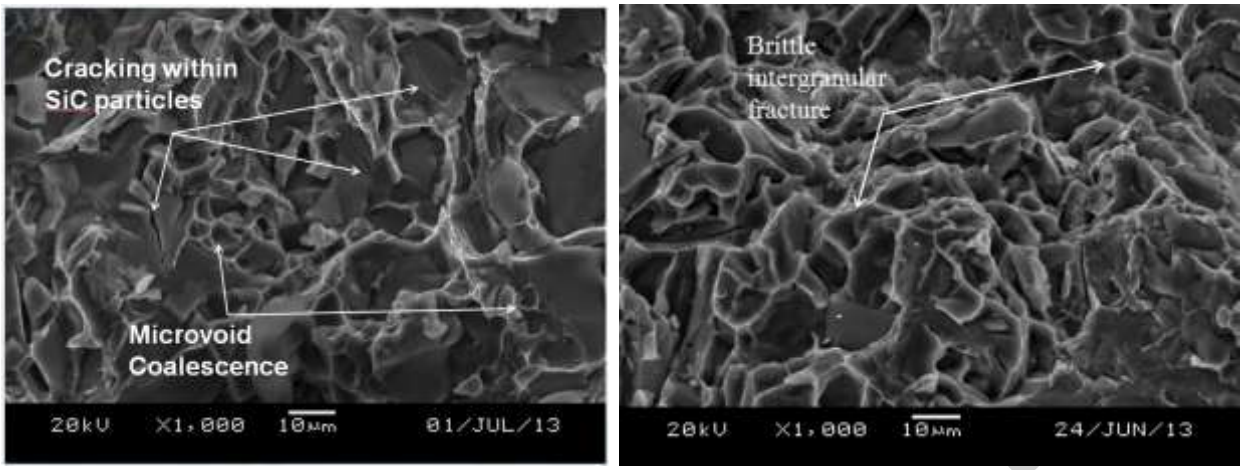

Figure 10. Scanning electron micrograph of the fracture surface of a) 304/Al-SiC-55P system, b) A36/Al-SiC-30P system.

Figure 11 illustrates specific stress strain curves for the following systems surrounded by 0.500" steel: 304/Al-Al_2O_3 46P, 304/Al-SiC 55P, A36/Al-Al_2O_3 46P, and A36/Al-SiC 55P. Evident from the figure, the systems which contain 304 SS have substantially higher strain to failure than the systems which are surrounded by A36 steel. The reinforcement type and volume percentage don't seem to have a large effect on the stress strain behavior indicating the strain of the composite system is mostly steel dependent.

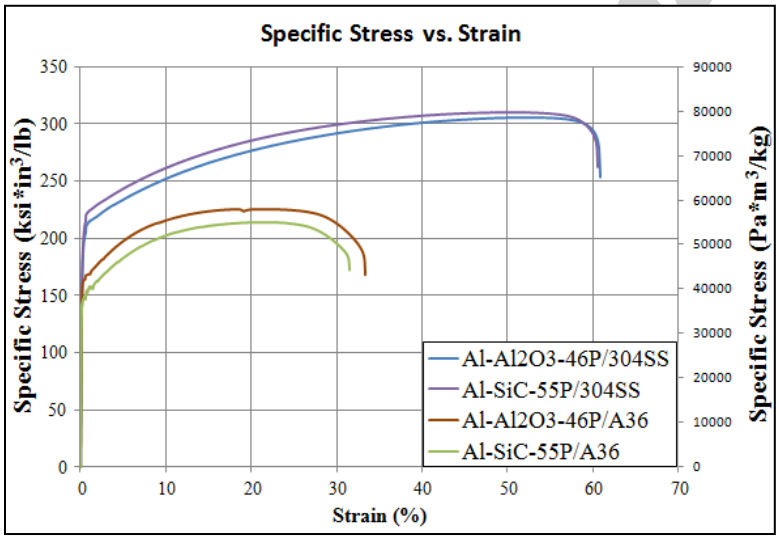

Figure 11. Specific stress-strain curves for macro composite materials systems (0.500" steel OD condition).

As evident from figure 12, each macro composite materials system exhibits improvement in % elongation (ductility) above the rule of mixture prediction at some steel shell thickness. The condition which appears to be most consistent in improving the ductility for all systems is the 14.1% MMC (0.500" steel shell) case. As expected, a larger volume of steel shell applies a higher confining stress onto its core compared with a thinner shell, which is consistent with the

neutron diffraction results. The residual stress caused by confinement in these cases suppresses void generation in the matrix resulting in an overall increase in the ductility of the system.

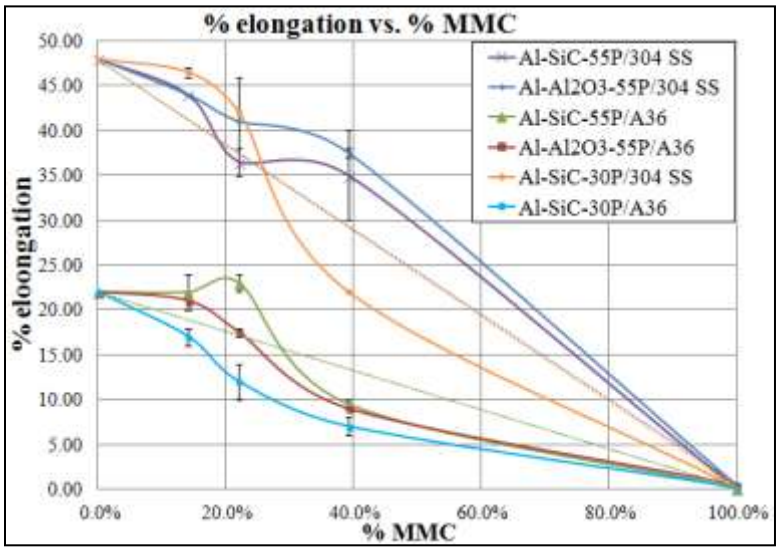

Figure 12. % Elongation vs. % MMC for each macro composite materials system.

4. Conclusions

Neutron diffraction can be used as an accurate and reliable method for measuring bulk residual tensile and compressive stresses within the steel encapsulated metal matrix composites. Low magnitude residual stresses within the steel are observed in the A36/Al-SiC systems which exhibit a low CTE mismatch between outer steel and MMC core. Conversely, the steel in the 304SS/Al-SiC systems have significantly higher residual stresses due to a large CTE mismatch between adjacent materials.

The confinement of the 0.626" 304SS on the Al-SiC MMC results in a 50 % more compressive stress in both the matrix and the reinforcement as compared with the same system surrounded by A36. The 1.0 inch thick surrounding steel results in a residual compressive stress in the MMC core approximately 15 % greater than the 0.626 inch steel for the 304/Al-SiC system. The higher CTE mismatch offered by the 304 SS vs. the A36 steel surrounding the Al-Al_2O_3 46P system results in over 100 % increases in tension in the steel and nearly 100% increase in compression in the Al_2O_3.

Over 20% improvement in specific yield stress is observed in the 304/Al-SiC 55P and 304/Al-Al_2O_3 46P systems due to improved load transfer and cracking of the reinforcement particles resulting from the steel confinement. Minor improvements of approximately 5-10 % are observed for specific ultimate tensile stress for the two systems: 304/Al-SiC 55P and 304/Al-Al_2O_3 46P for the 0.500" and 0.400" steel diameter conditions.

Each macro composite materials system exhibits improvement in % elongation compared with the rule of mixture predictions. Furthermore the thickest steel diameter, 0.500", results in the largest and most consistent improvement in the % elongation across all systems.

Acknowledgements

This work was partially funded by cooperative Agreement # W911NF-11-2-0040 between M Cubed Technologies Inc. and the US Army Research Laboratory (ARL), APG, MD.

This project was supported in part by an appointment to the Research Participation Program at the US ARMY Research Laboratory administered by the Oak Ridge Institute for Science and Education (ORISE).

This project was supported in part by the SMART Scholarship for Service Program.

This project was supported in part by the II-VI Foundation.

The authors declare no conflicts of interest.

References

[1] K. M. Shorowordi, T. Laoui, A. S. M. A. Haseeb, J. P. Celis, and L. Froyen, "Microstructure and interface characteristics of B4C, SiC and Al2O3 reinforced Al matrix composites: A comparative study," *J. Mater. Process. Technol.*, pp. 738–743, 2003.

[2] E. Taban, J. E. Gould, and J. C. Lippold, "Characterization of 6061-T6 aluminum alloy to AISI 1018 steel interfaces during joining and thermo-mechanical conditioning," *Mater. Sci. Eng. A*, pp. 1704–1708, 2010.

[3] A. Mazahery and M. Ostadshabani, "Investigation on mechanical properties of nano-Al2O3-reinforced aluminum matrix composites," *J. Compos. Mater.*, vol. 45, no. 24, pp. 2579–2586, 2011.

[4] G. B. V. Kumar, C. S. P. Rao, N. Selvaraj, and M. S. Bhagyashekar, "Studies on Al6061-SiC and Al7075-Al2O3 Metal Matrix Composites," *J. Miner. Mater. Charact. Eng.*, vol. 9, no. 1, pp. 43–55, 2010.

[5] D. L. McDanels, "Analysis of stress-strain, fracture, and ductility behavior of aluminum matrix composites containing discontinuous silicon carbide reinforcement," *Metall. Trans. A*, vol. 16, no. 6, pp. 1105–1115, 1985.

[6] I. A. Ibrahim, F. A. Mohamed, and E. J. Lavernia, "Particulate reinforced metal matrix composites - a review," *J. Mater. Sci.*, vol. 26, no. 5, pp. 1137–1156, 1991.

[7] D. J. Lloyd, "Particle reinforced aluminium and magnesium matrix composites," *International Materials Reviews*, vol. 39, no. 1. International Materials Review, pp. 1–23, 1994.

[8] D. S. Liu and J. J. Lewandowski, "The effects of superimposed hydrostatic pressure on deformation and fracture: Part I. Monolithic 6061 Aluminum," *Metall. Trans. A*, vol. 24, no. 3, pp. 601–608, 1993.

[9] D. S. Liu and J. J. Lewandowski, "The effects of superimposed hydrostatic pressure on deformation and fracture: Part II. Particulate-reinforced 6061 composites," *Metall. Trans. A*, vol. 24, no. 3, pp. 609–615, 1993.

[10] P. Karandikar *et al.*, "Processing of Hybrid Structures Consisting of Al-Based Metal Matrix Composites (MMCs) with Metallic Reinforcement of Steel or Titanium," in *TMS*, 2013, p. 20.

[11] P. Karandikar, E. M. Klier, M. Watkins, B. Mcwilliams, and M. Aghajanian, "Al/Al2O3 Metal Matrix Composites (MMCs) and Macrocomposites for Armor Applications," 2013.

[12] M. A. Prashant Karandikar, Matthew Duke, Allyn McCormick, "Net-Shape Al-B4C Metal

Matrix Composites (MMCs) for High Specific Stiffness and Neutron Absorption Applications." John Wiley & Sons, Inc., Hoboken, NJ, pp. 683–689, 2013.
[13] H. Zhang, K. T. Ramesh, and E. S. C. Chin, "High strain rate response of aluminum 6092/B4C composites," *Mater. Sci. Eng. A*, vol. 384, no. 1–2, pp. 26–34, 2004.
[14] S. Fudger, E. Klier, K. Prashant, B. Mcwilliams, and C. Ni, "Mechanical Properties of Steel Encapsulated Metal Matrix Composites," in *Advanced Composites for Aerospace, Marine, and Land Applications ll*, 2015, pp. 121–136.
[15] T. M. Holden, *Practical Residual Stress Measurement Methods*. Wiley, 2013.
[16] M. E. Fitzpatrick, M. T. Hutchings, and P. J. Withers, "Separation of Macroscopic, Elastic Mismatch and Thermal Expansion Misfit Stresses in Metal Matrix Composite Quenched Plates from Neutron Diffraction Measurements," *Acta mater*, vol. 45, no. 12, pp. 4867–4876, 1997.
[17] "Non-destructive testing - Standard test methods for determining residual stresses by neutron diffraction," *ISO/TS*, vol. 7, 2005.
[18] G. Bruno *et al.*, "Residual stress analysis in aerospace MMC materials by neutron diffraction," *Appl. Phys. A Mater. Sci. Process.*, pp. 1701–1703, 2002.
[19] R. Levy-Tubiana, A. Baczmanski, and A. Lodini, "Relaxation of thermal mismatch stress due to plastic deformation in an Al/SiCp metal matrix composite," *Mater. Sci. Eng. A*, pp. 74–86, 2003.
[20] G. Bruno, R. Fernández, and G. González-Doncel, "Gauge volume effects in residual stress determination by neutron diffraction: The strength differential effect in metal matrix composites," *Mater. Sci. Eng. A*, pp. 100–108, 2006.
[21] M. Vogelsang, R. J. Arsenault, and R. M. Fisher, "An in situ HVEM study of dislocation generation at Al/SiC interfaces in metal matrix composites," *Metall. Trans. A*, vol. 17, no. 3, pp. 379–389, 1986.
[22] M. H. Rahman and H. M. M. Al Rashed, "Characterization of silicon carbide reinforced aluminum matrix Composites," in *Procedia Engineering*, 2014.
[23] F. Tang, "The microstructure-processing-property relationships in an Al matrix composite system reinforced by Al-Cu-Fe alloy particles," Iowa State, 2004.
[24] M. C. T. Inc., "Metal Matrix Composites Aluminum alloy reinforced with ceramic particles," 2016. [Online]. Available: mmmt.com.
[25] "Panadyne." [Online]. Available: http://www.panadyne.com/. Accessed September 2015.
[26] "CoorsTek." [Online]. Available: https://www.coorstek.com/. Accessed September 2015.
[27] J. J. Lewandowski, D. S. Liu, and C. Liu, "Observations on the effects of particulate size and superposed pressure on deformation of metal matrix composites," *Scr. Metall. Mater.*, vol. 25, no. 1, pp. 21–26, 1991.